IOP Conf. Series: Materials Science and Engineering **361** (2018) 012015 doi:10.1088/1757-899X/361/1/012015

Experimental Study on Failure Mechanism of Advanced High Strength Steels in Air Bending Process

N Pornputsiri and K Kanlayasiri

Department of Industrial Engineering, Faculty of Engineering, King Mongkut's Institute of Technology Ladkrabang, Bangkok 10520, Thailand.

E-mail : natthasak_idt@hotmail.com

Abstract. This research investigated the failure phenomena and underlying damage mechanisms in small curvature bending and spring-back angles of two advanced high strength steel (AHSS) sheets (TRIP780 and DP980). The study also examined the effect of the bending angle on the failure mechanism. In the analysis, this research utilized an optimal microscope (OM), scanning electron microscope (SEM) and energy-dispersive X-ray spectroscope (EDX). The research findings indicated that the bending force and the bending angle were positively correlated and that the spring-back and bending angles were inversely correlated. On the failure mechanism, at the 45 ° bending angle, the initial crack was identified on the outer region of the LD-rolling DP980 sheet, while no visible crack emerged for the TD-rolling TRIP780 until arriving at the 60 ° bending angle, indicating that, by comparison, the former possessed the lowest bendability and the latter the highest.

1. Introduction

The structural lightweight, energy saving and safety requirements of the automotive industry contribute to the search for steels with high strength and good formability**.** In response, numerous attempts have been made and one viable solution is advanced high strength steels **(**AHSS**).** The enhanced strength however affects the formability of the steel into complex-shape parts. The AHSS are typically of multiphase steels whose microstructures comprise diverse phases, e.g. the dual phase **(**DP**)** and transformation induced plasticity **(**TRIP**)** steels [1]. To ascertain the industrial applicability of the DP and TRIP steels, it is necessary that the effects of their microstructures on the bendability and failure mechanisms be thoroughly investigated. The bendability of metallic sheets refers to the limit of the forming process accomplished without failure. The bending limit could be defined as the amount of elongation on the outer surface of the bending zone, from which a minimum bending radius is deduced [2]. Furthermore, the limit is subject to a variety of parameters, including the ratio of sheet thickness to tool radius, material properties, surface and microstructure of the metal sheet.

It is well known that the fabrication history has a significant effect on bendability and must be included failure mechanisms in order to achieve accurate predictions of forming limits. Nakataki et al [3] investigated the bendability of dual-phase AHSS metal sheets and it was documented that the microstructure of these steels could be refined and homogenized for the bendability improvement. Kaupper and Merklein [4] proposed the failure phenomena and underlying damage mechanisms associated with the small curvature bending of AHSS using a novel comprehensive optical strain-based characterization technique. R'eche et al [5] studied the failure mechanism in air-bending of

TRIP steel sheet and the results showed that the initial cracks occurred on the outer bent surface (roof) of the metal sheet. Despite the ubiquity and severity of metal failure in the industrial production, prior research has largely focused on the relationship between the bending angle and the damage mechanism at the expense of several other contributing factors of the metal failure. In other words, there exists no research that attempts to explain the relationship of the metal microstructure, rolling direction and bending angle to the bendability and the failure mechanism of the metal sheet has ever been carried out.

This current research has investigated the relationships between the bending angle and the bending force; and between the bending and spring-back angles of the TRIP780 and DP980 AHSS steel sheets under the traverse (TD) and longitudinal (LD) rolling directions. The effect of the bending angle on the failure mechanism was also determined. In addition, an optimal microscope (OM), scanning electron microscope (SEM) and energy-dispersive X-ray spectroscope (EDX) were deployed in the analysis.

2. Materials and experimental procedure

2.1. Materials

This research experimented with two types of AHSS sheets of identical thickness (1mm): the transformation induced plasticity (TRIP780) and dual phase (DP980) steels. Table 1 tabulates their tensile mechanical properties determined using the uniaxial tensile test at room temperature.

Table 1. Mechanical property at room temperature.

Material	Yield Stress (MPa)	Ultimate Tensile Stress (MPa)	Total Elongation (%)
TRIP780	589	983	24.7
DP980	638	1017	19

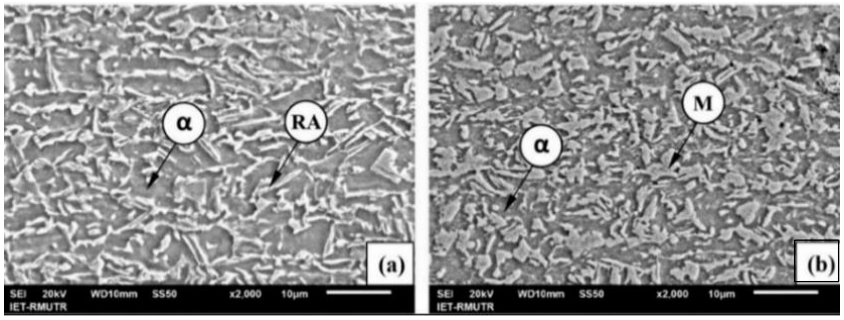

Figure 1. Initial microstructure of investigated steels (a) TRIP780 and (b) DP980.

In this research, the microstructure and chemical composition were respectively analyzed using SEM. Figure 1(a) illustrates the TRIP780 microstructure comprising the island-like retained austenite (RA) phases embedded in the ferrite matrix (α). Meanwhile, Figure 1(b) depicts the DP980 microstructure consisting of ferrite matrix (α) in which the martensitic phase (M) is dispersed in the form of islands.

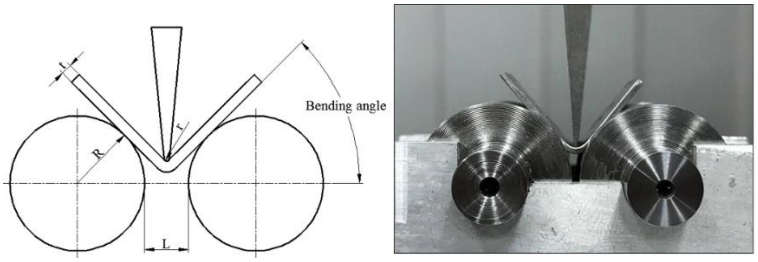

Figure 2. The schematics of the pure-bending experimental setup.

2.2. Experimental procedure

Figure 2 illustrates the pure-bending plane-strain experimental setup to investigate the failure mechanisms of the TRIP780 and DP980 steel sheets using the air bending test as per the ISO 7438:2010 standard. The punch (r) and roller (R) radii were respectively 0.25mm and 10mm. The metal sheets were 12mm in width (b), 30mm in length (l) and 1.0mm in thickness (t).

In the operation, the punch pressed downward while the support set remained stationary. The experiments were carried out by varying the bending angles in a 15° increment from 0° to 75° under the room temperature and without lubrication condition. The post-bending failure mechanisms were determined using photography technology by which the outer surface bent area was first investigated using a Digital Single Lens Reflex (DSLR) camera (CANNON, EOS 80D EF-S) and a Light Optical Microscope (LOM) (JENCO, GL7-290) to identify the initial crack. The specimens were then polished and etched prior to undergoing the macro-scale microstructure inspection using a 50X Optical Microscope (OM) (OLYMPUS, BX 60 M) to investigate the cross-sectional crack and crack propagation. The cross-sectional micro-scale failure mechanisms and the chemical composition at the bent area (or fracture surface) were further determined using SEM (JEOL, JSM-6510 LV) and EDX (OXFORD, X-MAX IE-350).

3. Experimental Results and Discussion

3.1. Relationships between the bending angle and spring-back angle

This part investigates the effects of the bending angle on the bendability of the TRIP780 and DP980 experimental metal sheets, given the two rolling directions (i.e. TD and LD).

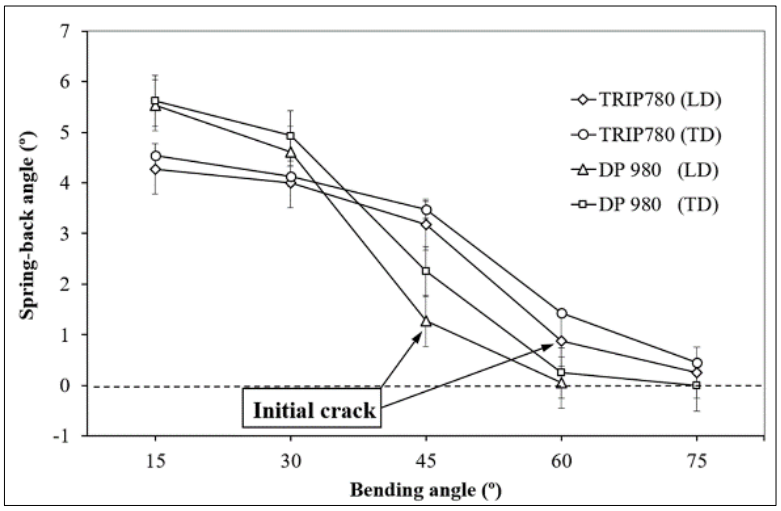

Figure 3. Relationships between the spring-back angle and bending angle of the DP and TRIP steels in the longitudinal and transverse rolling directions.

Figure 3 depicts the spring-back angles relative to the various bending angles (0 °-75 °) and the rolling directions. The experimental results showed that the spring-back angles were inversely correlated with the bending angles, whereby the spring-back angles decreased with increase in the bending angles. By comparison, the spring-back angles relative to the bending angles were greatest for the TD-rolling TRIP780 metal sheet, suggesting the highest bendability, followed by TRIP780LD, DP980TD and DP980LD. The relationship between the spring-back and the bending angle, in these phenomena, the large of plastic deformation at higher bending angle on the bending area, this decreases the elongation property which in turn induces a lower spring-back angle and can be expressed in equation (1), where K is the ultimate tensile strength, θ is the bending angle, ρ is the position of the neutral axial, υ is the Poisson ratio, ω is the die gap, E is the Young's modulus and t is the thickness [6].

$$\frac{\Delta\theta}{\theta} = \frac{3K_{\rho}(1-\upsilon^2)_{(1+4t/\omega)}}{Et} \quad (1)$$

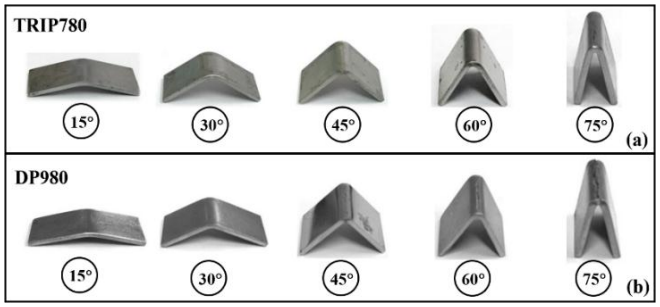

Figure 4. The LD-rolling failure mechanisms under various bending angles: (a) TRIP780 (b) DP980 steels.

Figure 4 compares the LD-rolling failure mechanisms under the bending angles of 15 °-75 ° of the TRIP780 and DP980 steel sheets. In figure 4(a), the failure (i.e. cracks) started to appear on the roof of the TRIP780 sheet under the 75 ° bending angle condition and the crack propagation increased with increase in the bending angle but with no complete separation. Meanwhile, in figure 4(b), at the 45 ° bending angel, numerous crack lines emerged on the roof of DP980 and deteriorated as the bending angle increased. The total separation of the DP980 specimen occurred once the bending angle reached 75 °.

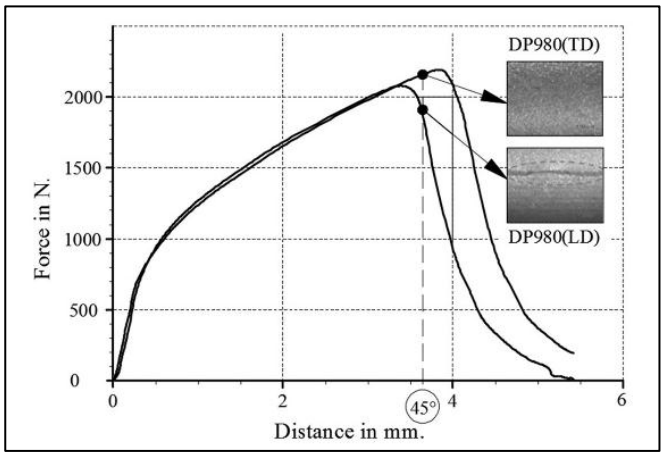

Figure 5. The relationship between the punch depth, rolling directions and bending force at the roof of DP980 sheet.

Figure 5 illustrates the relationship between the punch depth, rolling directions and bending force at the outer bent surface (roof) of DP980 sheet. In the figure, the bending force increased with the

punch depth (mm) for both rolling directions. The bending force belonging to the LD-rolling DP980 started to decline approaching (before) the 45 ° bending angle. On the other hand, in the traverse-rolling direction, the bending force declined shortly after arriving at the 45 °bending angle. The forces continued to decrease as the punch depth increased. The findings indicated that the TD-rolling DP980 outperformed the LD-rolling counterpart with regard to the bendability and strength. The experimental findings are consistent with the theory of anisotropic materials [7] in which the traverse-rolling direction (TD) material exhibits greater bendability than that of the longitudinal-rolling direction (LD).

3.2. Failure Mechanisms

The failure mechanisms of the TRIP780 and DP980 steel sheets in the longitudinal direction (LD) of rolling were investigated and compared. As previously mentioned, the LD rolling is more susceptible to cracking and thereby the study focus. Figure 6 depicts the cross-sectional SEM failure mechanism of the LD-rolling TRIP780 steel under the 75 ° bending angle condition, where (A), (B) and (C) represent the outer, central and inner regions. Under the 75 °bending angle, the failure was noticeably pronounced from the edge of the outer region to the central region, while small cracks appeared in the inner region. Upon closer inspection, a small crack however emerged and could be detected in the LD-rolling TRIP780 steel under the bending angle of 60 °, as illustrated in figure 7.

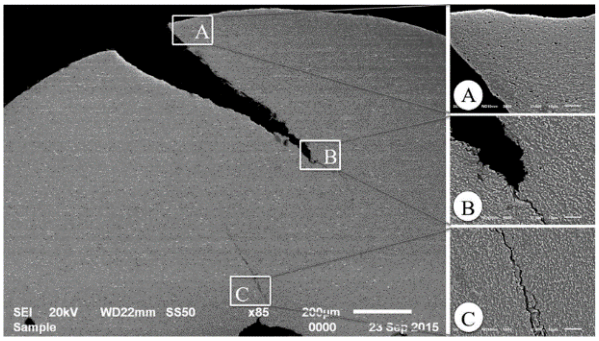

Figure 6. The cross-sectional SEM failure mechanism of the LD-rolling TRIP780 steel with the 75 ° bending angle: (A) the outer, (B) central, (C) inner regions.

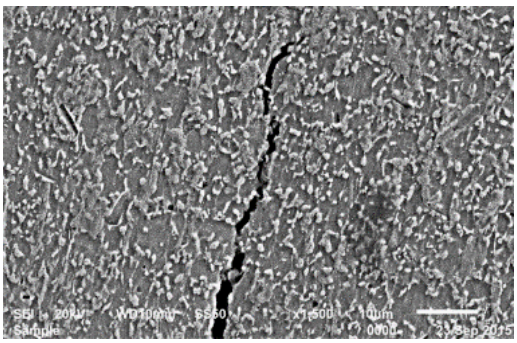

Figure 7. The cross-sectional OM of LD-rolling TRIP780 in which the initial crack appeared on the inner region with the 60° bending angle.

Figure 7 depicts the cross-sectional optical microscopy of the LD-rolling TRIP780 metal sheet under the 60 ° bending angle condition. In the figure, despite the outward compressive stress-induced hairline fracture on the inner region [8], the overall bendability of the metal sheet was minimally restricted. This phenomenon is attributable to a delayed crack propagation on this particular region relative to that of the tensile stress-induced outer region.

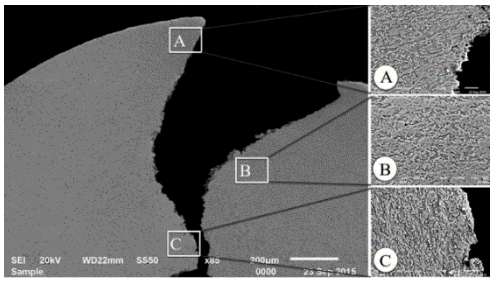

Figure 8. The cross-sectional SEM failure mechanism of the LD-rolling DP980 steel with the 75 ° bending angle: (A) the outer, (B) central, (C) inner regions.

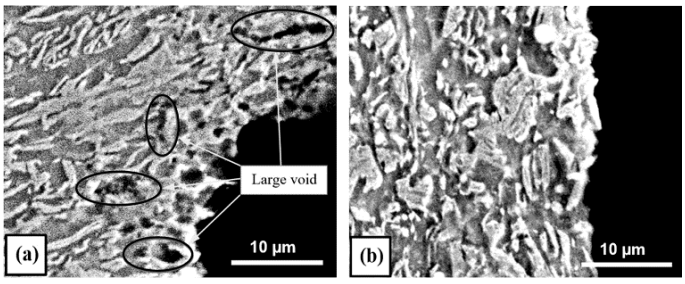

Figure 9. The SEM images of DP980 under the 75 ° bending angle: (a) the outer and (b) inner regions.

Figure 8 illustrates the cross-sectional SEM failure mechanism of on the outer (A), central (B) and inner (C) regions of the LD-rolling DP980 steel under the 75 ° bending angle, where a complete separation took place. In the figure, the crack propagation was of 45 ° in relation to the punch, consistent with Rèche et al [5]. Specifically, the phase in the outer region (A) was elongated along the outermost edge of the metal sheet, while there was minimal change in the martensitic phase in the central region (B). In the inner region (C), the shape of the martensitic phase altered as per the punch direction. In fact, the initial cracks on the DP980 steel sheet emerged under the bending angle 45° condition (Figure 4), with the extent of failure more pronounced on the outer than inner region. With the increase in the bending angle, the dual-directional cracks propagated to the central region of the metal sheet. A total separation of the specimen materialized at the 75° bending angle. Figure 9(a) and (b) are the magnified SEM images on the outer regions and the inner region, respectively, of the DP980 steel sheet under the 75 ° bending angle condition. In figure 9(a), voids of varying sizes (i.e. macro- and micro-voids) were present on the outer and central regions where ferrite and martensite interface, with the significant proportion residing on the outer region. The crack propagation on both the outer and central regions proceeded in the direction of the macro-voids inward (i.e. toward the inner region). Meanwhile, in figure 9(b), the crack propagation on this region (i.e. inner region) was attributable to the compressive pressure. Due to the compressive pressure, no void was detected on the inner region. The experimental results with regard to the initial crack of both metal sheet types are consistent with Pathak et al [9] and Zhao et al [10]. The results are in good agreement.

4. Conclusions

This experimental research has investigated the relationships between the bending angles and the bending force; and between the bending and spring-back angles of two types of advanced high strength steel (AHSS) sheets (TRIP780 and DP980) under two rolling direction conditions (traverse (TD) and longitudinal (LD)). The study also determined the effect of the bending angle on the failure mechanism of the metal sheets. The findings revealed that the bending force and the bending angle were positively correlated. Specifically, the bending force of TRIP780 steadily rose with increase in the bending angle under both rolling directions. Meanwhile, the bending force of the LD-rolling DP980 increased and decreased approaching the 45 ° bending angle while that of the TD-rolling DP980 increased and declined shortly after arriving at the 45 ° bending angle. Interestingly, the bending force of the LD-rolling DP980 reversed to zero at the 75 ° bending angle, the point at which a total separation occurred. On the other hand, the spring-back and bending angles were inversely correlated. The experiments revealed that the TD-rolling TRIP780 and LD-rolling DP980 sheets respectively had the largest and smallest spring-back angles under all the experimental bending angles. Nevertheless, the spring-back angle of the LD-rolling DP980 became zero at the 60 ° bending angle. On the failure mechanism, at the 45 ° bending angle, the initial crack could be detected on both the inner and outer regions of the LD-rolling DP980 sheet; and on the inner region of the TD-rolling TRIP780 sheet. The crack was more severe when the bending angle reached 60 ° for the TD-rolling TRIP780.

References

[1] Zhao P, Chang Y, Hu P and Wu Y 2016 *J. Mat. Pro. Tech.* 228 68–75.
[2] Rèche D, Sturel T, Bouaziz O, Col A and Gourgues-Lorenzon A F 2011 *Mater. Sci. Eng. A.* 528 5241–5250.
[3] Nakataki Y, Tsuyama S and Hosoya Y 2013 *Tetsu. to. Hagané* **99** 245-253.
[4] Kaupper M and Merklein M 2013 *CIRP. Ann. Manuf. Techn.* 62 247–250.
[5] R'eche D, Besson J, Sturel T, Lemoine X and Gourgues-Lorenzon A F 2012 *Int. J. Mech. Sci.* 57 43–53.
[6] Fei D and Hodgson P 2006 *Nucl .Eng .Des.* 236 1847–1851.
[7] Panich S, Uthaisangsuk V, Suranuntchai S and Jirathearanat S 2014 *Mater. Sci. Eng. A.* 592 207-220.

[8] Aslam I, Li B, McClelland Z, Horstemeyer S J, Ma Q and Wang P T 2014 *Mater. Sci. Eng. A.* 590 168–173.
[9] Pathak N, Butcher C, Worswick M J, Bellhouse E and Gao J 2017 *Materials* 10, 346; doi:10.3390/ma10040346.
[10] Zhao Z, Huang S, Dan W, Zhang W and Li S 2017 *Mater. Sci. Eng. A.* 695 80–91.

Acknowledgements
The authors would like to express sincere gratitude to King Mongkut's Institute of Technology Ladkrabang (KMITL)'s Faculty of Engineering for the financial support.